

# Warm Pool and Cold Tongue El Niño Events as Simulated by the GFDL 2.1 Coupled GCM

JONG-SEONG KUG

*Korea Ocean Research and Development Institute, Ansan, South Korea*

JUNG CHOI AND SOON-IL AN

*Department of Atmospheric Sciences, Yonsei University, Seoul, South Korea*

FEI-FEI JIN

*School of Ocean and Earth Science and Technology, University of Hawaii at Manoa, Honolulu, Hawaii*

ANDREW T. WITTENBERG

*NOAA/Geophysical Fluid Dynamics Laboratory, Princeton, New Jersey*

(Manuscript received 16 June 2009, in final form 21 September 2009)

## ABSTRACT

Recent studies report that two types of El Niño events have been observed. One is the cold tongue (CT) El Niño, which is characterized by relatively large sea surface temperature (SST) anomalies in the eastern Pacific, and the other is the warm pool (WP) El Niño, in which SST anomalies are confined to the central Pacific. Here, both types of El Niño events are analyzed in a long-term coupled GCM simulation. The present model simulates the major observed features of both types of El Niño, incorporating the distinctive patterns of each oceanic and atmospheric variable. It is also demonstrated that each type of El Niño has quite distinct dynamic processes, which control their evolutions. The CT El Niño exhibits strong equatorial heat discharge poleward and thus the dynamical feedbacks control the phase transition from a warm event to a cold event. On the other hand, the discharge process in the WP El Niño is weak because of its spatial distribution of ocean dynamic field. The positive SST anomaly of WP El Niño is thermally damped through the intensified evaporative cooling.

## 1. Introduction

The richness of the coupled air–sea phenomena has been recognized in the tropical Pacific more than in any other place (Jin 2001). Many recent studies have argued that there exists more than one type of El Niño [or El Niño–Southern Oscillation (ENSO)] based on spatial distributions of SST (Larkin and Harrison 2005a,b; Ashok et al. 2007; Weng et al. 2007; Kao and Yu 2009; Kug et al. 2009b; Yeh et al. 2009) or physically separated modes (Neelin et al. 1998; Jin et al. 2003; Bejarano and Jin 2008). The former group found the strongest evidence that there is a type of El Niño event that has

action centers of atmospheric and oceanic variables located primarily over the central Pacific and warm pool region, which is distinguished from the traditional canonical feature of ENSO (or the conventional El Niño) (Rasmusson and Carpenter 1982; Wallace et al. 1998). They also reported that these events appear to be more frequent and persistent occurrences during recent decades (Ashok et al. 2007; Kug et al. 2009b; Yeh et al. 2009). So far, inconsistent nomenclature has been used for this new type of El Niño event, such as “date line El Niño” (Larkin and Harrison 2005a,b), “El Niño Modoki” (Ashok et al. 2007; Weng et al. 2007), “central Pacific El Niño” (Kao and Yu 2009; Yeh et al. 2009), and “warm pool El Niño” (Kug et al. 2009b). Although there is no consensus in terminology, we will use the term “warm pool (WP) El Niño,” because this study is basically extension of Kug et al. (2009b).

---

*Corresponding author address:* Prof. Soon-Il An, 262 Seongsanno, Seodaemun-gu, Seoul 120-749, South Korea.  
E-mail: sian@yonsei.ac.kr

Each of the aforementioned studies emphasized somewhat different aspects of these El Niño events, examining the same phenomenon from slightly different points of view. We extracted the following major features:

- (i) There is a distinct interannual SST variation over the central Pacific that differs from the conventional El Niño;
- (ii) the SST variation over the central Pacific has displayed stronger variance in recent decades;
- (iii) the global impact of this new type El Niño is significant and quite different from that of the conventional El Niño;
- (iv) zonal advective feedback is the key process for evolution of the WP El Niño events, while the thermocline feedback is more important for that of the cold tongue (CT) El Niño (e.g., Jin and An 1999; An and Jin 2001).

Though the observational composite analyses showed how the two types differ, the analyses are limited by the small number of observations. To overcome this limitation, numerical models can be a useful tool for understanding natural phenomena and for testing hypotheses. In particular, several studies have used the state-of-the-art coupled GCMs to understand ENSO dynamics (Yu and Mechoso 2001; Guilyardi et al. 2003, 2004; Kim et al. 2008; Kug et al. 2009c) and the relationship between ENSO and other climate phenomena (Yu et al. 2002; Gualdi et al. 2003; Wu and Kirtman 2004a,b; Lau and Nath 2004; Kug et al. 2006a,b). In this study, we analyze a long-term simulation of the Geophysical Fluid Dynamics Laboratory (GFDL) Climate Model version 2.1 (CM2.1) coupled GCM (CGCM; Delworth et al. 2006; Wittenberg et al. 2006). The GFDL CGCM is capable of simulating both types of El Niño phenomena, the characteristics of which are similar to those observed.

Section 2 provides a brief description of the GFDL coupled GCM utilized in this study. In section 3, we describe the two types of El Niño events simulated by the coupled model. Their evolution and transition processes are depicted in section 4. The summary and discussion are given in section 5.

## 2. Model

### a. Description of the model

This study employs the GFDL CM2.1 long-term simulation. The ocean component is ocean model version 3.1 (Gnanadesikan et al. 2006; Griffies et al. 2005), which is based on Modular Ocean Model version 4 (MOM4) code. The resolution is 50 vertical levels and a  $1^\circ \times 1^\circ$  horizontal grid telescoping to  $\frac{1}{3}$  meridional spacing near the equator. The vertical grid spacing is a constant 10 m over the

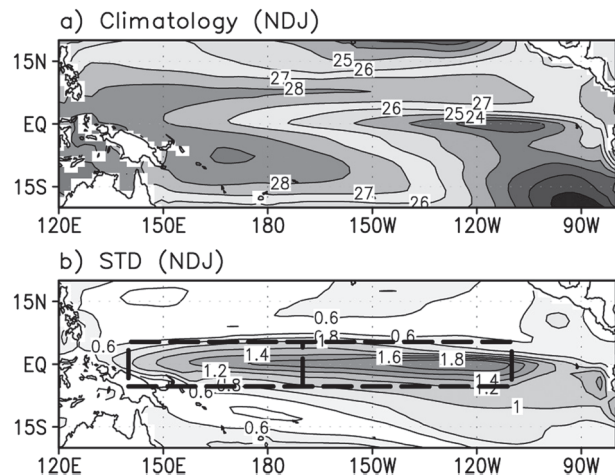


FIG. 1. (a) Climatology of SSTs ( $^{\circ}\text{C}$ ) over the tropical Pacific during ND(0)J(1) from CGCM. (b) Standard deviation of ND(0)J(1) SST anomalies ( $^{\circ}\text{C}$ ). The dashed boxes in (b) indicate the modified Niño-3m region (right box;  $5^{\circ}\text{S}$ – $5^{\circ}\text{N}$ ,  $170^{\circ}$ – $110^{\circ}\text{W}$ ) and Niño-4m region (left box;  $5^{\circ}\text{S}$ – $5^{\circ}\text{N}$ ,  $140^{\circ}\text{E}$ – $170^{\circ}\text{W}$ ).

top 220 m. The atmospheric component is the GFDL atmospheric model (AM2p13). The resolution is 24 vertical levels and  $2^{\circ}$  latitude by  $2.5^{\circ}$  longitude grid spacing. The dynamic core is based on a finite volume (Lin 2004). Air–sea fluxes are computed based on 1-h intervals. For a detailed model description, refer to Delworth et al. (2006) and Wittenberg et al. (2006). In this study, we used a 500-yr preindustrial simulation, with fixed values for atmospheric composition, land cover, and insolation based on data for the year 1860. The initial conditions were computed by starting from Levitus and then running for 200 years subject to the 1860 forcing. The data are available in the phase 3 of the Coupled Model Intercomparison Project (CMIP3) archives (available online at <https://esg.llnl.gov:8443/index.jsp>).

Figure 1 shows the SST winter mean climatology and standard deviation of the simulated interannual SST anomaly in November–January (NDJ) periods, at the peak phase of El Niño events. Overall, the simulated climatological SST and interannual variability are comparable to those in observation. However, the equatorial cold SST bias and the equatorial westward SST gradient are somewhat stronger in the western and central Pacific because of the further westward penetration of the cold tongue. These systematic biases are observed in most of CGCMs (AchutaRao and Sperber 2002; Davey et al. 2002; Hannachi et al. 2003; Latif et al. 2001).

In general, the present model overestimates the interannual variability of SST, which is found not only in the eastern Pacific but also in the central-western Pacific. In addition, the standard deviation is smaller in the equatorial eastern Pacific near the coast and the west coast

of South America compared to those in the observation. This indicates that the location of the strong variability in this model shifts farther westward than observed, which is a common problem in most CGCMs (AchutaRao and Sperber 2002; Hannachi et al. 2003; Latif et al. 2001). Presumably, this is related to the westward extension of the cold tongue. The detailed descriptions of the performance of the model, especially over the tropical Pacific, are found in Wittenberg et al. (2006).

### b. Distinctions between WP El Niño and CT El Niño

To define two types of El Niño events, we use modified Niño-3 and Niño-4 SST indices because the climatological cold tongue extends farther west than observational data would suggest, and because ENSO variability is also shifted slightly to the west in the model (Fig. 1). Wittenberg et al. (2006) noted that the simulated patterns of tropical Pacific SST, wind stress, and precipitation variability are displaced longitudinally by  $20^{\circ}$ – $30^{\circ}$  west of the observed pattern. Based on this information, we defined new indices. We defined Niño-3m SST as the averaged SST over  $5^{\circ}\text{S}$ – $5^{\circ}\text{N}$ ,  $170^{\circ}$ – $110^{\circ}\text{W}$  and Niño-4m SST as the averaged SST over  $5^{\circ}\text{S}$ – $5^{\circ}\text{N}$ ,  $140^{\circ}\text{E}$ – $170^{\circ}\text{W}$  (Fig. 1b). Note that the area thus defined is shifted about  $20^{\circ}$  longitude to the west compared to the conventionally defined area. Based on the two indices, all El Niño events are initially selected when either of the two indices is greater than  $0.5^{\circ}\text{C}$  during NDJ. A total of 205 El Niño events were selected. The distribution for Niño-3m and Niño-4m SST anomalies (SSTA) is shown in Fig. 2. We found that the ratio between the two indices is markedly varied, indicating that the spatial distribution of SST cannot be characterized by any one single pattern (i.e., one type of El Niño). We classified the 205 El Niño events as WP or as CT. El Niño events with a Niño-4m SSTA greater than the Niño-3m SSTA were considered WP and those with a Niño-3m SSTA greater than the Niño-4m SSTA were labeled CT. We acknowledge that this division into only two groups is a limitation. Some events exhibiting similar magnitudes for Niño-3m and Niño-4m indices, though in reality mixed, were still placed in one of the two groups. Based on our definitions, a total of 121 events were classified as WP El Niño events and 84 as CT El Niño events.

### 3. Warm pool El Niño and cold tongue El Niño

To compare the two types of El Niño events, we performed a composite analysis. In this section, we will first focus on the features of the mature phase (NDJ). Their evolution will be discussed in the next section.

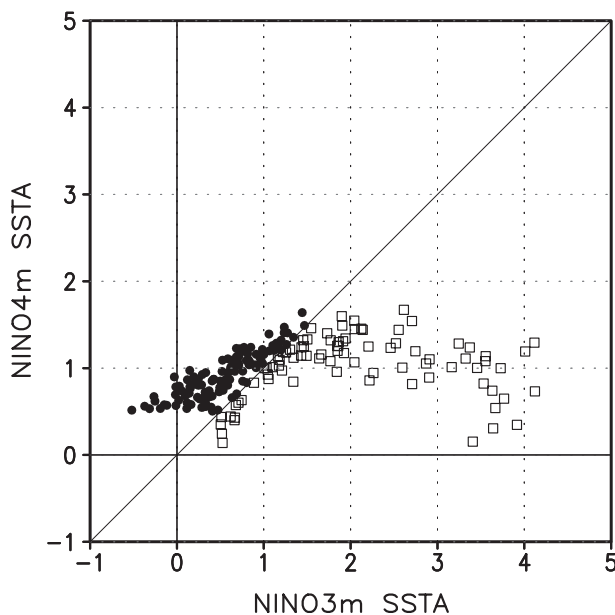


FIG. 2. Scatterplots in Niño-3m–Niño-4m SST anomaly plane. Open-square (closed circle) marks indicate the CT El Niño (WP El Niño).

Figure 3 shows SST composites of the CT El Niño and WP El Niño events. It is clear that the SST anomalies in both composites have quite different patterns in terms of location and amplitude. The SST pattern of the WP El Niño is distinct from that of the CT El Niño. In the case of the CT El Niño, large SST anomalies appeared mainly over the eastern equatorial Pacific. The maximum SST anomaly is about  $2.5\text{ K}$  and is located at  $120^{\circ}\text{W}$ . The location of the SSTA center is consistent with that of the observed CT El Niño, but the SST anomalies are elongated farther west in the Pacific, and there is no negative SST over the western equatorial Pacific, which differs from observations (See Fig. 3c of Kug et al. 2009b). Note that most features in the composite are statistically significant, as determined by the  $t$  test.

On the other hand, SST anomalies of the WP El Niño events mainly appeared west of the international date line (maximum located around  $160^{\circ}\text{E}$ ), which is a shift to the west of about  $30^{\circ}$  compared to that of the observed WP El Niño (see Fig. 3c of Kug et al. 2009b). The magnitude of the SST anomaly was about  $1.0\text{ K}$ , which is smaller than that of the CT El Niño. Also not in agreement with observations, the negative SST anomaly over the equatorial western Pacific was not observed in the WP El Niño composite. In spite of some dissimilarity, it seems the model does simulate the major distinctions between the two types of El Niño events that have been reported in the observational data. This implies that the model has the ability to simulate both

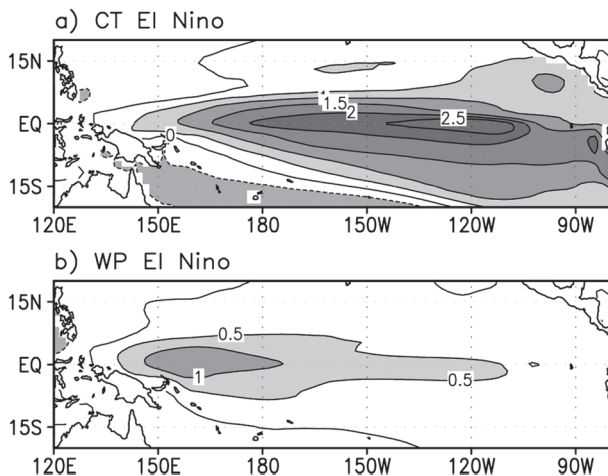


FIG. 3. SST anomaly ( $^{\circ}\text{C}$ ) composite of the (a) CT El Niño and (b) WP El Niño during ND(0)J(1).

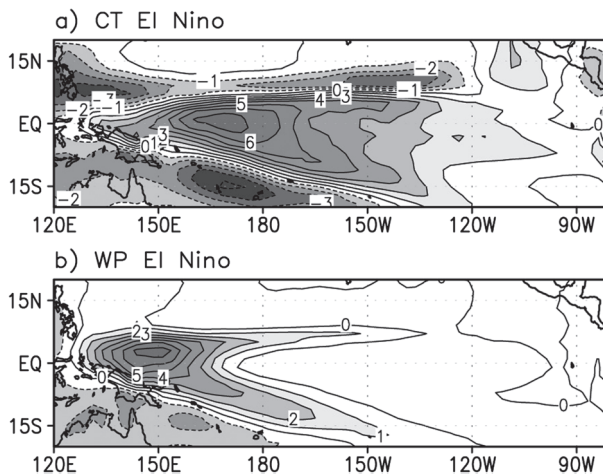


FIG. 4. As in Fig. 3, except for precipitation ( $\text{mm day}^{-1}$ ).

types of observed El Niño events, providing an opportunity to explore further, through analysis of the model, the underlying dynamics of the observed two types of El Niño.

Since each type of El Niño is characterized by a distinctive SST pattern, we would expect that the associated atmospheric responses might also differ. Figure 4 shows precipitation composites of the two types of El Niño events. The precipitation patterns in both composites are distinctively different. Precipitation anomalies associated with the CT El Niño are zonally elongated over the entire equatorial Pacific basin, with a center located near 170°E, whereas the precipitation anomalies associated with the WP El Niño are confined to the western Pacific, with a center at 150°E. This is consistent with the pattern of SST shown in Fig. 3b. Overall, the location of the precipitation is consistent with the region where the zonal gradient of the SST anomalies is strong (cf. Ropelewski and Halpert 1987).

In addition, negative off-equatorial precipitation anomalies are clearly shown in the CT El Niño composite, which is known as the western Pacific anomaly pattern associated with the conventional El Niño (Weisberg and Wang 1997; Wang et al. 1999). The precipitation anomalies induce a cyclonic wind shear and shallowing thermocline in the off-equatorial western Pacific. These observational features are captured well in the CT El Niño composites of the present model. However, in the WP El Niño composite, the western Pacific pattern is not found. Namely, there is no significant precipitation anomaly in the off-equatorial region of the Northern Hemisphere (NH). So, their off-equatorial responses of low-level wind and thermocline depth are quite different from those of the CT El Niño. Instead,

large off-equatorial precipitation anomalies are apparent over the Indian Ocean in the WP El Niño composite (not shown).

Another interesting finding is that the WP El Niño composite shows positive off-equatorial precipitation anomalies with relatively minimal precipitation at the equator to the east of the international date line, which is different from that of the CT El Niño. This is possibly because the equatorial total SST is not enough to generate precipitation (Vecchi et al. 2006; Lengaigne and Vecchi 2009). These differences in horizontal structures of precipitation anomalies between the two types of El Niño are quite consistent with those observed (Kug et al. 2009b). However, the model tends to simulate more hemispherically symmetrical features, possibly because of the double-ITCZ problem (Wittenberg et al. 2006).

It is not clear yet why the two types of El Niño have a different off-equatorial precipitation response in both the simulation and observation. For example, it is known that the distinct pattern in the meridional precipitation structure is related to the meridional gradient SST (Lengaigne and Vecchi 2009). However, there is no significant difference in the meridional extent of SST. The present model simulates the equatorial cold tongue to be located far west, as shown in Fig. 1, and thus the equatorial SST is much colder than the off-equatorial SST in the central Pacific. Even during the WP El Niño, the equatorial SST is still colder than the off-equatorial SST. On the other hand, the CT El Niño SST is large enough to reverse the meridional SST gradient. The warmer equatorial SST intensifies atmospheric convection, which may lead to off-equatorial dryness through an intensified sinking motion. These processes should be further studied with more detailed analysis.

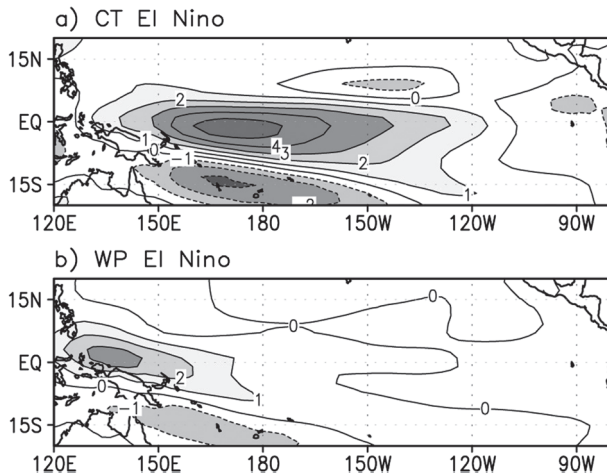


FIG. 5. As in Fig. 3, except for zonal wind at 925 hPa ( $\text{m s}^{-1}$ ).

It is also interesting that the maximum precipitation anomaly in CT El Niño composite is comparable to that in WP El Niño composite, though the SSTA magnitude of the CT El Niño events is 2.5 times larger than that of the WP, as shown in Fig. 3. This is because the central Pacific SST anomalies are much more efficient in inducing atmospheric convections than are the eastern Pacific SST anomalies because of the background wind convergence and warmer background SSTs (Wang 2000). This makes the global impact of the WP comparable to the CT in spite of its relatively small SST anomaly. Different patterns of anomalous convection can lead to differences in the atmospheric circulation, and one may expect distinctive atmospheric teleconnections (e.g., Hoerling et al. 1997; An et al. 2007). The distinctive global impacts of the two types of El Niño were reported recently in several studies (Larkin and Harrison 2005a,b; Ashok et al. 2007; Weng et al. 2007; Ashok et al. 2009). The present model also simulates different teleconnection patterns for the two types of El Niño events (not shown).

Figure 5 shows composites of a zonal wind anomaly at 925 hPa. In the case of the CT El Niño, there are strong anomalous westerlies over the western-central Pacific. In contrast, the center of the anomalous zonal wind is located to the west and its zonal scale is relatively smaller in the WP El Niño composite. These longitudinal distributions of wind are consistent with the distribution of precipitation, indicating that both types of El Niño events are strongly coupled air–sea phenomena. Also of note, in the CT El Niño composites the precipitation and zonal wind are almost in phase in terms of the zonal location, while the zonal wind is shifted to the west by about 20° compared to the precipitation in the WP El Niño composites, which are closer to the Gill-

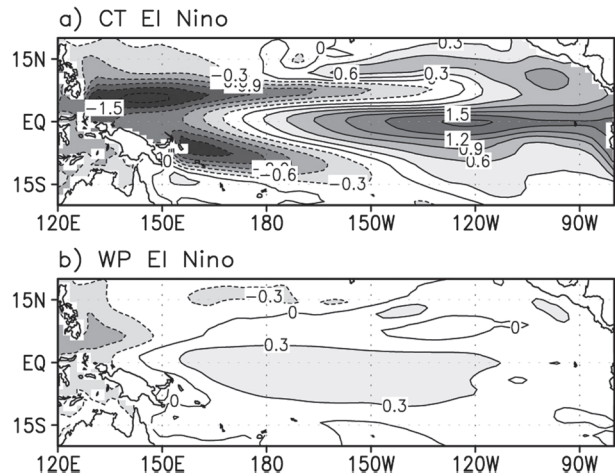


FIG. 6. As in Fig. 3, except for heat content (K).

type solution when any specified basic state is not prescribed (Gill 1982). The phase relationship between heating and zonal wind response is an open question yet to be solved (cf. Clarke 1994). We shall leave this for further study.

The anomalous low-level wind generates an anomalous oceanic state in the tropical Pacific. Figure 6 shows heat content anomalies associated with the two types of El Niño events. Heat content anomalies are calculated by integrating ocean temperature anomalies from the surface to a depth of 300 m. For the CT El Niño composite, the seesaw pattern is clear, namely that the thermocline is deepening (shoaling) over the eastern (western) Pacific. It is also evident that the maximum of heat content anomaly is located in the off-equatorial region over the western Pacific because of the cyclonic wind shear (Wang et al. 1999). Note that changes in heat content can be analogous to changes in the thermocline depth. The deepening thermocline induces a strong anomalous warm vertical advection by mean upwelling over the eastern Pacific (Battisti 1988; Kang et al. 2001; An and Jin 2001). Thus, the positive SST anomaly is dominant in the eastern Pacific. Also, the steep zonal slope of the thermocline leads to a strong discharge of equatorial heat content to the off-equatorial regions by the poleward geostrophic currents, leading to a transition from El Niño to La Niña (Jin 1996, 1997a,b).

On the other hand, in the case of the WP El Niño, the positive heat content anomaly is located over the central Pacific, and its maximum near 160°W coincides with a nodal point of zonal wind anomaly, as shown in Fig. 5b. We found that the magnitude of the heat content anomaly is small compared to that of the CT El Niño. In addition, the climatological thermocline depth over the equatorial central Pacific is relatively deep compared to

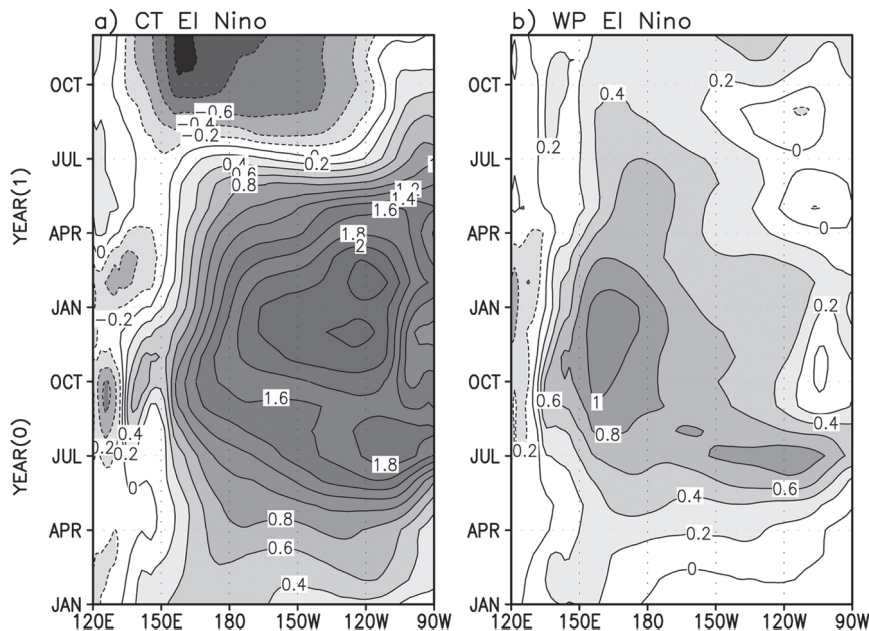


FIG. 7. Time-longitude section of the equatorial ( $5^{\circ}\text{S}$ – $5^{\circ}\text{N}$ ) SST anomaly (K) for (a) CT El Niño and (b) WP El Niño.

that in the eastern Pacific. Thus, the subsurface temperature below the mixed layer in the tropical central Pacific is less sensitive to change of the thermocline depth. In this regard, the heat content anomaly in the tropical central Pacific may not efficiently produce the warm SST anomaly. However, the zonal gradient of climatological SST is strong over the central Pacific, so the zonal advective feedback can play a dominant role in developing the WP El Niño.

The difference in zonal distributions of heat content anomalies between the two types of El Niño events can lead to a difference in the phase transition. The strong east–west contrast in the heat content anomaly leads to a strong discharge, while the heat content anomalies associated with a WP El Niño do not support this strong discharge. This difference can lead to different forms of evolution, as discussed in the next section.

#### 4. Evolution of the two types of El Niño events

To depict the temporal evolution of both types of El Niño event, the time-longitude cross section of SST along the equator is shown in Fig. 7. In the case of the CT El Niño, the SST anomaly begins developing in early spring, and there are two peak seasons: summertime and wintertime over the eastern Pacific. It is conceivable that the double peaks of the eastern Pacific SST are related to too strong a semiannual cycle (Wittenberg et al. 2006). The SST anomaly rapidly develops between April and June. Note that the SST pattern of the CT El Niño

events is quite stationary. However, the WP El Niño composite shows somewhat different evolution. The surface warming starts relatively late and a rapid development happens over the central Pacific during the period July–September. Interestingly, there is a short-term SST peak over the eastern Pacific during the summer. It seems that the summer peak in the eastern Pacific SST in the both CT and WP El Niño composites is unique in the present model; it is rarely found in the observational data. This SST warming is tightly locked to the seasonal cycle and is closely related to the short-term fluctuation of the equatorial zonal current (not shown). However, details regarding the dynamic processes that drive this warming are not clear.

A striking difference in the temporal evolution between the two types of El Niño events appeared in the transition period. The CT El Niño composite shows a rapid phase transition to La Niña that is already developed at the end of the following year, while the WP El Niño slowly dampened by the end of the following year. This phase transition in the CT El Niño is related to the discharge process of the equatorial heat content.

As seen in Fig. 6, the maximum sea level in the WP El Niño composite is located at  $160^{\circ}\text{W}$ . Therefore, the zonal gradient of the sea level is eastward, to the west of the maximum, and westward to the east of the maximum. The eastward (westward) gradient leads to poleward (equatorial) transport of heat content (or warm water) by meridional divergence (convergence) of the geostrophic currents (Jin 1997a,b; Meinen and McPhaden 2000, 2001;

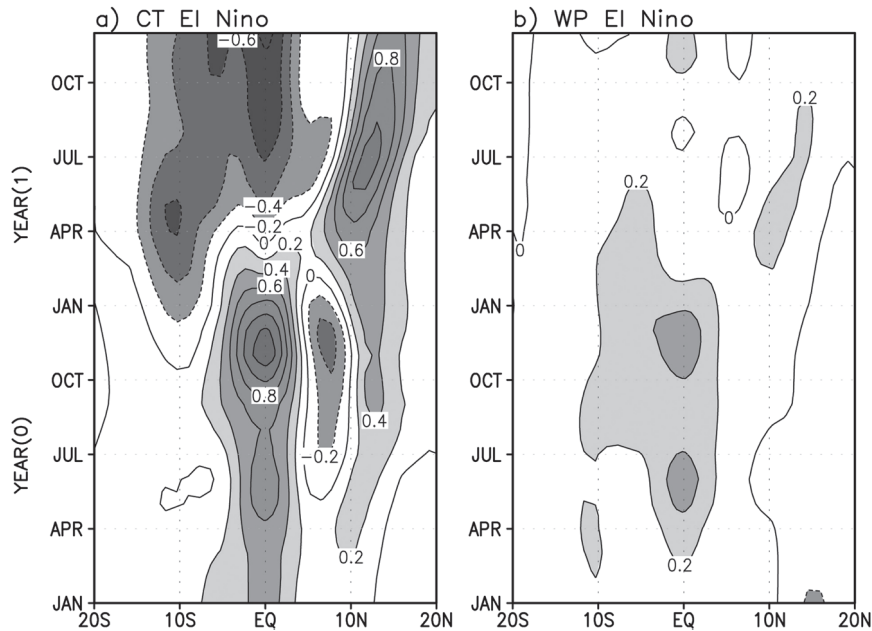


FIG. 8. Time-latitude section of the zonal-mean ( $160^{\circ}\text{E}$ – $90^{\circ}\text{W}$ ) heat content anomaly (K) for (a) CT El Niño and (b) WP El Niño.

Kug et al. 2003). Thus, both components mitigate each other so that the net total heat content in the equatorial region is zero. This indicates that the discharge process of the equatorial heat content is not efficient in the case of the WP El Niño so that the discharge process suggested by Jin (1997a,b) cannot serve as the phase-transition mechanism. Note that the eastward gradient of heat content is quite strong in the case of the CT El Niño. Therefore, the discharge process associated with the CT El Niño effectively leads to a transition from warm phase to cold phase, following the recharge oscillator paradigm (Jin 1997a,b).

To examine the heat content exchanges between the equator and off-equator regions, the evolution of zonal-mean heat content over the Pacific basin ( $160^{\circ}\text{E}$ – $90^{\circ}\text{W}$ ) is shown in Fig. 8. According to the recharge oscillator theory (Jin 1997a,b), a positive anomaly of equatorial heat content leads to a positive SST anomaly over the eastern Pacific. In the CT El Niño composite, it seems that the heat content anomaly leads to a SST anomaly by several months. During the developing phase, strong positive heat content prevails in the equatorial region, and the negative heat content prevails north of the equator. After the peak phase of the CT El Niño, the equatorial heat content is rapidly discharged so that a strong negative anomaly appears. At the same time, a positive zonal-mean heat content anomaly develops north of the equator. Note that the heat content anomaly over the south of the equator has the same sign as the

equatorial anomaly. The heat content exchanges associated with the CT El Niño happen between the equator and north of the equator as described by Kug et al. (2003). Kug et al. (2003) argued that the southward shift of the center of zonal wind from the equator leads to the hemispheric asymmetric mass exchanges. As shown in Fig. 5a, the center of the zonal wind anomaly is slightly shifted to the south, supporting their finding.

The evolution of zonal-mean heat content is quite different in the case of the WP El Niño. Most significantly, the discharge of the equatorial heat content (i.e., the drain of the zonal-mean equatorial heat content) is quite weak during the decaying phase. The heat content anomaly does not become negative after the WP El Niño peak phase. Therefore, there is no transition from the El Niño to the La Niña because of the anomalous shoaling of the equatorial thermocline, which tends to promote a cold event in the case of the CT El Niño, and this negative heat content operates slowly to damp the warming anomaly, restoring normal conditions, as shown in Fig. 7b. This weak discharge effect is related to the zonal location of wind stress and the corresponding heat content distribution as discussed earlier.

To explore the discharge process further, we compared the zonal-mean meridional transport of the seawater. We calculated the meridional transport by integrating the meridional current from the surface to a depth of 300 m. Figure 9 shows the evolution of the zonal-mean meridional transport for the two types of El Niño events. In

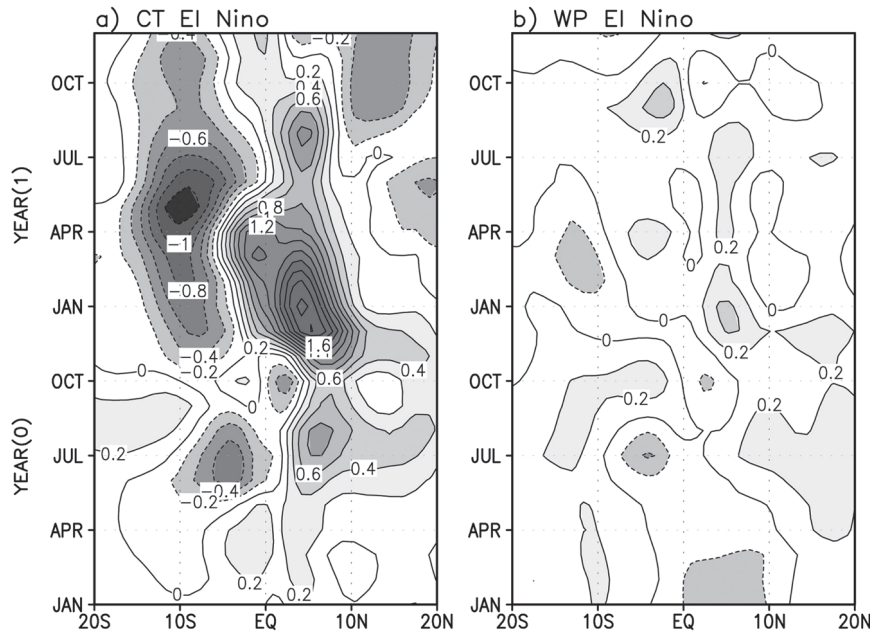


FIG. 9. As in Fig. 8, except for ocean meridional current averaged from surface to 300-m depth ( $\text{m s}^{-1}$ ).

the CT El Niño composite, there are clear poleward transports in both hemispheres, indicating a divergence in the equatorial region. The meridional transport is strongest during the peak phase of the CT El Niño when the equatorial zonal gradient of the heat content is positive. Note that the meridional transport toward NH is stronger than that toward the Southern Hemisphere (SH), which is consistent with the asymmetric distribution of heat content shown in Fig. 8a. On the other hand, the WP El Niño composite does not show strong meridional transport. Though there is divergence at the peak phase of the WP El Niño, the magnitude is quite weak. Presumably, it is related to the zonal distribution of heat content shown in Fig. 6b, which leads to almost no net meridional transport. Again, this is because the meridional transport that occurred in the equatorial eastern Pacific is compensated by that in the equatorial western Pacific. The discharge process is related to the zonal location of the SST anomalies and the resultant wind and heat content distribution. By showing individual CT and WP El Niño events (Fig. 10) rather than a composite, we extract a general relationship between the discharge process and the zonal location of the SST anomaly. The abscissa in Fig. 10 represents the location of the SSTA centroid ( $X$ ), which is defined by

$$X = \frac{\int \text{SSTA}(x)x \, dx}{\int \text{SSTA}(x) \, dx}, \quad (1)$$

where  $\text{SSTA}(x)$  denotes the equatorial SSTA averaged over  $5^{\circ}\text{S}$ – $5^{\circ}\text{N}$  during El Niño peak phase [ $\text{ND}(0)\text{J}(1)$ ] and  $x$  denotes the longitude. The zonal integration was executed over  $120^{\circ}\text{E}$ – $90^{\circ}\text{W}$ . This definition is also used by Kug et al. (2009a). Discharge is estimated from the difference of the equatorial zonal-mean heat content between the El Niño peak phase [ $\text{ND}(0)\text{J}(1)$ ] and one year later [ $\text{ND}(1)\text{J}(2)$ ]. Figure 10a clearly demonstrates that the discharge process depends on the zonal location of the SSTA. As the SSTA center locates farther eastward, the discharge becomes more effective. The correlation coefficient is 0.64, which is significant to a 99% confidence level. In particular, the relationship is almost linear when the SSTA center is located to the east of the international date line. Figure 10b shows the relationship between the discharge process and the zonal location of the zonal wind anomaly at 925 hPa. The center of the zonal wind anomaly is calculated as in SSTA. A linear relationship between two variables is also clear. The correlation coefficient is 0.58, which is significant to a 99% confidence level. That is, the discharge becomes more effective as the center of the zonal wind anomaly moves eastward. The zonal distribution of the equatorial thermocline is highly dependent on the distribution of zonal wind. This provides further evidence of a distinctive difference in the discharge process between two types of El Niño as a result of the zonal locations of SSTA and wind anomalies.

The different discharge processes are associated with different physical processes in the two types of El Niño.

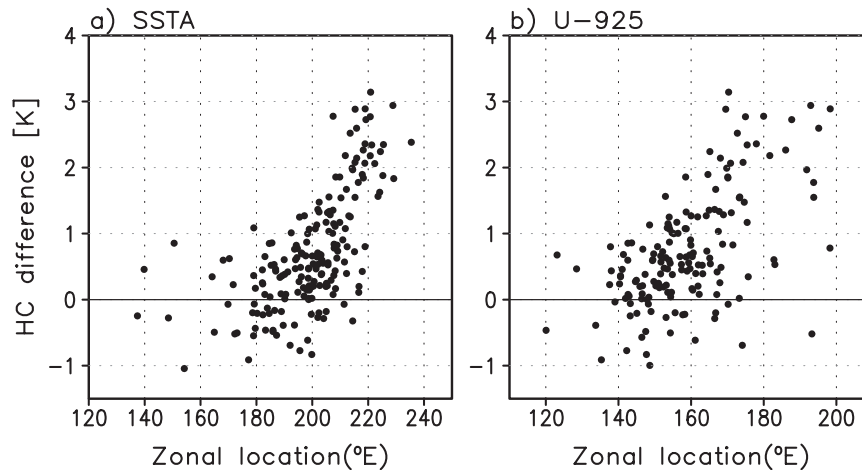


FIG. 10. Scatterplots between the discharge of the heat content and the zonal location of the (a) SST anomaly and the (b) zonal wind at 925 hPa. A detailed description is in the text.

The equatorial SST anomalies associated with ENSO develop by two major pathways: (i) thermocline feedback and (ii) zonal advective feedback (Picaut et al. 1997; Jin and An 1999; Kang et al. 2001; An and Jin 2001). Kug et al. (2009b) noted that thermocline feedback is a key process for the CT El Niño, while zonal advective feedback is a key to the WP El Niño. Here, we also see the relative importance of the two feedback process for the two types of events. We performed a budget analysis of the mixed-layer temperatures. The thermocline feedback and zonal advective feedback terms are defined as follows:

$$\text{Thermocline feedback: } -\overline{w} \frac{\partial T'}{\partial z}$$

$$\text{Zonal advective feedback: } -u' \frac{\partial \overline{T}}{\partial x},$$

where the overbar and prime indicate monthly climatology and anomaly, respectively. Variables  $u$  and  $T$  indicate zonal current and oceanic temperature averaged over the mixed layer (fixed at 50 m). Vertical velocity ( $w$ ) is calculated at the bottom of the mixed layer. For simplicity, each term is area averaged over the Niño-3m and Niño-4m regions (except that meridional boundaries of 2°S–2°N are used) for the CT El Niño and WP El Niño, respectively. Also, we delineated the period of development [March (0) to November (0)] and the period of decay [February (1) to October (1)].

Figure 11 shows the contributions of each term in the developing and decaying periods. In the case of the CT El Niño, both thermocline feedback (light-gray bar) and zonal advective feedback (dark-gray bar) play a critical role in both development and decay of the eastern Pacific surface warming, which is consistent with the obser-

vatational studies on conventional El Niño events (Kang et al. 2001). In particular, the thermocline feedback plays a dominant role during the decay phase. After the El Niño peak phase, there is a strong discharge of heat content, which leads to rapid shoaling of the thermocline over the eastern Pacific. The shallow thermocline induces subsurface cooling, and the climatological upwelling pumps cold water from the subsurface to the surface, which leads to a strong cooling tendency in SST. The net heat flux (black bar) shows a negative SST tendency in both the development and decay phases, indicating that it always damps a positive SST anomaly. Note that the magnitude of the atmospheric heat flux is smaller than that of the dynamic cooling term in the decaying phase over Niño-3m region. In the Niño-4m region, the zonal advection is dominant during the developing period, while the vertical advection is dominant in the decaying period because of excessive discharge.

However, the WP El Niño composite shows quite different contributions of two feedback processes. In the period of decay, thermocline feedback exhibits a similar magnitude of positive SST tendency to that in the period of development, indicating that this feedback does not help much for the evolution of the WP El Niño. However, the positive tendency of the zonal advective feedback is significantly reduced in the period of decay, though its sign is still positive. It is interesting that the advection terms, including two feedback terms, do not show a significant negative tendency in the period of decay, while net heat flux is significantly changed, which is different from the CT El Niño composite. In other words, during the phase of development, the net heat flux is nearly zero, but it becomes a large negative tendency during the phase of decay indicating a strong damping effect. Since the net heat flux overwhelms the

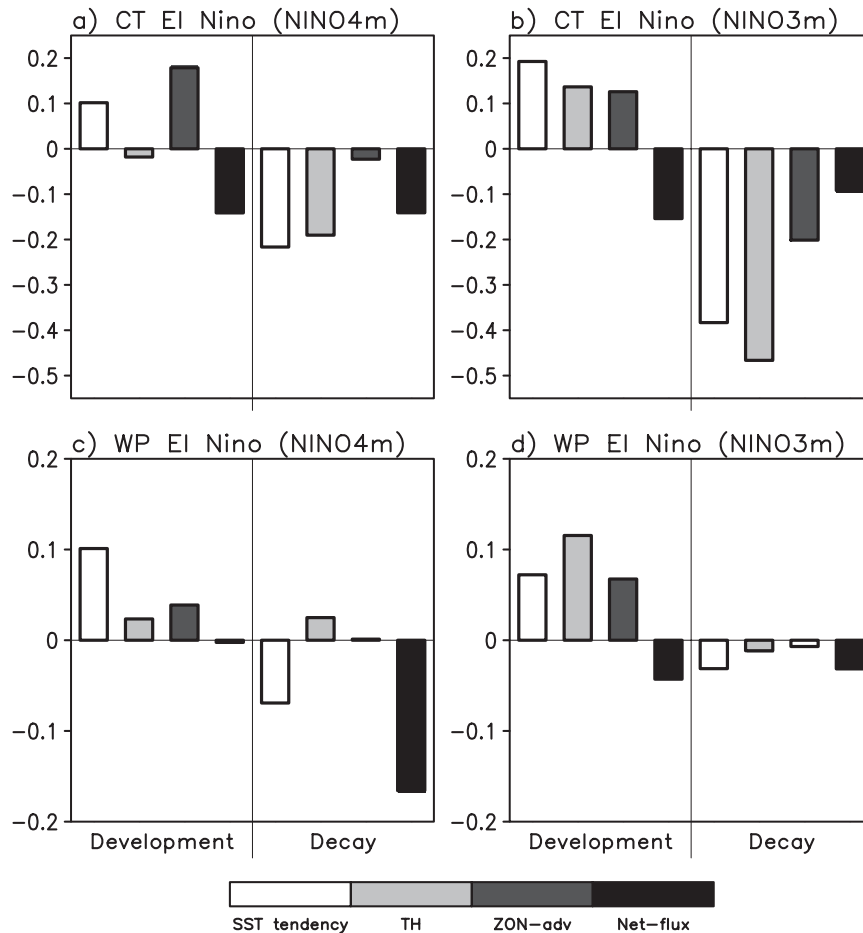


FIG. 11. SST tendency (open bar), SST tendency according to the thermocline feedback (light-gray bar), the zonal advective feedback (dark-gray bar), and net flux (black bar) for (a),(b) CT El Niño and (c),(d) WP El Niño ( $\text{K month}^{-1}$ ). Each magnitude is calculated over  $2^{\circ}\text{S}$ – $2^{\circ}\text{N}$ ,  $170^{\circ}$ – $110^{\circ}\text{W}$  [(b),(d) Niño-3m region] or  $2^{\circ}\text{S}$ – $2^{\circ}\text{N}$ ,  $140^{\circ}\text{E}$ – $170^{\circ}\text{W}$  [(a),(c) Niño-4m region]. Period of development (decay) is defined from March (0) to November (0) [from February (1) to October (1)].

advective heating by the zonal advective and thermocline feedbacks, the positive SST anomaly is damped to the climatological value but does not develop a negative SST.

It is very interesting that net heat flux in the Niño-4m region is nearly zero during the developing period of the WP El Niño, though the SST anomaly remains significantly positive. Figure 12 shows the contribution of each net heat flux for the CT and WP El Niño composites. It is clear that the latent heat flux anomalies are quite different. The CT El Niño exhibits a latent heat flux in the Niño-3m region with a strong negative tendency in the phase of development. In the Niño-4m region, the latent heat flux is relatively weak. On the other hand, the WP El Niño composite signal is very weak during the developing period. However, there is strong negative tendency by the latent heat flux in the decaying phase.

During the developing phase of the CT El Niño, the SST anomaly is positive and wind speed is reduced because of the anomalous westerly in the Niño-3m region. The positive SST anomaly intensifies the cooling effect of the latent heat flux by increasing ocean surface evaporation, while the reduced wind speed reduces the cooling effect of the latent heat flux by decreasing evaporation. Because the climatological SST is relatively cold and the climatological wind speed is relatively strong in the Niño-3m region, the intensification of latent heat flux due to change in the SST anomaly overwhelms the reduction of latent heat flux due to change in the wind speed, and thus anomalous cooling is induced by latent heat flux. In the decaying phase, however, the positive SST anomaly is changing to the negative SST anomaly because of the fast transition, and the time-averaged latent heat flux from 1 February to 1 October is nearly

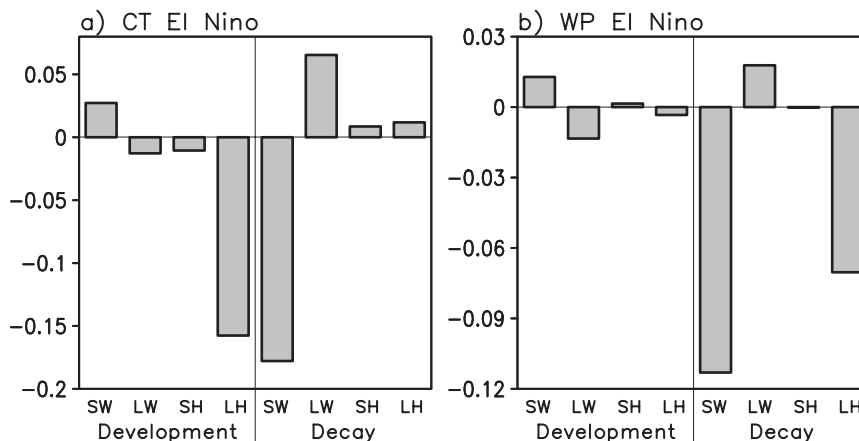


FIG. 12. SST tendency according to the net flux (Fig. 11) is separated by each flux term ( $\text{K month}^{-1}$ ). (left to right) Net shortwave flux (SW), net longwave flux (LW), sensible heat flux (SH), and latent heat flux (LH). CT El Niño (WP El Niño) cases are calculated over the Niño-3m (Niño-4m) region except for  $2^{\circ}\text{S}$ – $2^{\circ}\text{N}$ .

zero. On the other hand, in the Niño-4m region, the climatological SST is higher and wind speed is weak so that the effect due to change in the wind speed is relatively large. In this regard, nearly zero latent heat flux in the developing phase of the WP El Niño may be attributed to a cancellation between the increment of latent heat flux associated with increased SST and the decrement of latent heat flux associated with the decreased wind speed. However, the wind speed anomaly is significantly reduced during the decaying phase of the WP El Niño, and so no cancellation occurs, because of a strong negative tendency in the latent heat flux.

In the conventional El Niño, the reversal of the sign of the feedback terms between the developing and decaying periods resulted from the discharging process and the associated sign reversal in the zonal-mean heat content (An et al. 1999; An and Jin 2001). An and Jin (2001) pointed out that the equatorial negative heat content generates equatorial westward geostrophic current and a shoaling thermocline, which leads to a negative SST tendency in the two feedback terms. However, the WP El Niño exhibits a very weak discharge and is even weakly positive in the decaying period (see Fig. 8b). Because the shoaling thermocline tendency is very slow as a result of the weak discharge in the decaying period, the SST decay due to atmospheric heat flux can be faster than subsurface cooling due to the shoaling thermocline, resulting in a positive tendency of thermocline feedback during the decaying period. In addition, the weak positive (or nearly zero) heat content cannot generate the westward current anomaly, so the zonal advection term does not have a negative tendency during the decaying period.

From the budget analysis, it is found that the dynamical feedback terms play an active role in the de-

velopment and decay of the CT El Niño because the recharge and discharge processes are dominant. Therefore, the dynamical feedback can lead to a clear phase transition from the warm phase to the cold phase, possibly indicating a self-sustained oscillatory mode. For the WP El Niño events, the zonal advective feedback plays a key role in the surface warming during the developing period, but the dynamical feedback terms do not play an important role in the phase transition because of the weak discharge process. Instead, surface warming tends to be thermally damped to the climatological value, and the cold event rarely follows in the next year.

## 5. Summary and discussion

In this study, we investigated two types of El Niño events in a preindustrial control simulation of the GFDL CM2.1 coupled GCM spanning about 500 years. Though their patterns shifted to the west because of the model mean bias compared to the observed, the present model simulates the major observed features of the two types of El Niño event very well. For example, the action centers in the atmospheric and oceanic variables are located over the central Pacific and warm pool regions in the WP El Niño, which is distinctively different from the CT El Niño. Also, the zonal scale for the WP El Niño is relatively small compared to that of the CT El Niño. A striking difference appeared in the transition processes of the two events. In the case of the CT El Niño, the discharge process is very strong and thus dynamic feedback controls the phase transition from warm event to cold event. On the other hand, the discharge process in the WP El Niño is very weak because of its spatial distribution, and it seems the surface warming induced

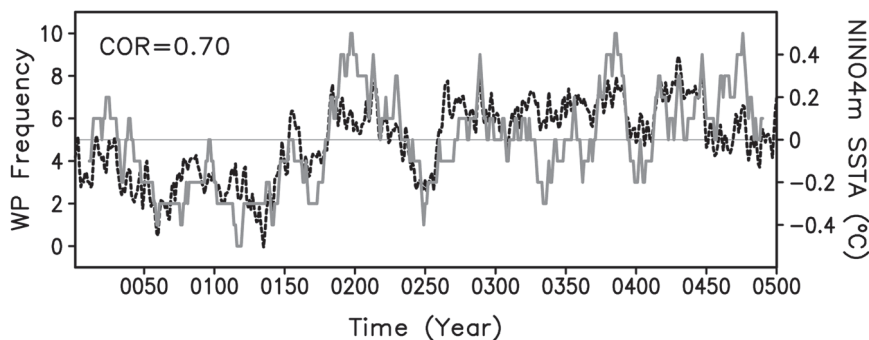


FIG. 13. Gray solid line indicates 20-yr moving WP El Niño frequency (number of occurrence). Black-dashed line is long-term mean Niño-4m SSTA with 20-yr moving slide.

by zonal advection slowly decays because of a thermal damping process.

Kug et al. (2009b) pointed out using the observational analysis that the cold events are not easily separated into WP and CT types because conventional La Niña events are already shifted to the west compared to the El Niño events. It is also found that the cold events simulated by the present CGCM are hardly separated into two types. In particular, we found their pattern is relatively close to those of the CT El Niño with the opposite sign (not shown). This implies the WP El Niño is more a stochastic event than an oscillatory phenomenon.

Because the WP El Niño events tend not to be accompanied by cold events after their termination, their occurrence and existence can modulate climate mean states in the tropical Pacific. In other words, frequent occurrences of the WP El Niño contribute to an accumulative warming of the mean state. In observational data, the occurrence of the WP El Niño is well matched with the warming period of the long-term SST (more than five years) over the central Pacific. For example, during the periods of 1990–95 and 2001–06, there are long-lived SST anomalies in the central Pacific. Their SST patterns are similar to that of the WP El Niño. In the model simulation, we found a similar tendency.

Figure 13 shows the occurrence frequency of the WP El Niño and long-term mean Niño-4m SSTA with a 20-yr moving slide. It is striking that the two variables are so closely related. The correlation coefficient is 0.70. That is, the frequency occurrence is related to the warmer state of the tropical decadal to interdecadal variability. There are two possible explanations for this clear relationship. First, the WP El Niño could be inducing the tropical decadal variability by means of a nonlinear rectification effect (Timmermann 2003; Rodgers et al. 2004; An et al. 2005; An 2009). Second, the basic state could be providing favorable conditions for the frequency occurrence of the WP El Niño. Because the

zonal advective feedback is a key process in the developing WP El Niño, the zonal gradient of the climatological SST may be related to the frequency of the WP El Niño events. If the mean SST over the western Pacific increases, it can provide favorable conditions for WP El Niño development. Also, atmospheric response to the given SST is strong when the background SST is warmer. That is why the magnitude of the precipitation response to the WP El Niño is comparable to that of the CT El Niño though the SST magnitudes are quite different. In this sense, the warmer mean surface conditions can provide favorable conditions for the occurrence of WP El Niño by providing strong air–sea coupling. Therefore, there are possible two-way interactions between WP El Niño events and decadal variability. However, the detailed dynamical process is not yet fully elucidated; we intend to further investigate this two-way interaction in the future.

*Acknowledgments.* J.-S. Kug is partly supported by KORDI (PE98445, PE98511, and PE98512). F.-F. Jin was supported by NSF Grants ATM-0652145 and ATM-0650552 and NOAA Grants GC01-229. S.-I. An was supported by the “National Comprehensive Measures against Climate Change” Program of the Ministry of the Environment, Korea (Grant 1600-1637-301-210-13), and by the Korean Research Foundation Grant funded by the Korean Government (MOEHRD, Basic Research Promotion Fund) (KRF-2007-313-C00784).

## REFERENCES

- AchutaRao, K., and K. R. Sperber, 2002: Simulation of the El Niño Southern Oscillation: Results from the Coupled Model Intercomparison Project. *Climate Dyn.*, **19**, 191–209.
- An, S.-I., 2009: A review of interdecadal changes in the nonlinearity of the El Niño–Southern Oscillation. *Theor. Appl. Climatol.*, **97**, 29–40.

- , and F.-F. Jin, 2001: Collective role of thermocline and zonal advective feedbacks in the ENSO mode. *J. Climate*, **14**, 3421–3432.
- , —, and I.-S. Kang, 1999: The role of zonal advection feedback in phase transition and growth of ENSO in the Cane-Zebiak model. *J. Meteor. Soc. Japan*, **77**, 1151–1160.
- , Y.-G. Ham, J.-S. Kug, F.-F. Jin, and I.-S. Kang, 2005: El Niño–La Niña asymmetry in the Coupled Model Intercomparison Project. *J. Climate*, **18**, 2617–2627.
- , J.-S. Kug, A. Timmermann, I.-S. Kang, and O. Timm, 2007: The influence of ENSO on the generation of decadal variability in the North Pacific. *J. Climate*, **20**, 667–680.
- Ashok, K., S. K. Behera, S. A. Rao, H. Weng, and T. Yamagata, 2007: El Niño Modoki and its possible teleconnection. *J. Geophys. Res.*, **112**, C11007, doi:10.1029/2006JC003798.
- , S. Iizuka, S. A. Rao, N. H. Saji, and W.-J. Lee, 2009: Processes and boreal summer impacts of the 2004 El Niño Modoki: An AGCM study. *Geophys. Res. Lett.*, **36**, L04703, doi:10.1029/2008GL036313.
- Battisti, D. S., 1988: Dynamics and thermodynamics of a warming event in a coupled tropical atmosphere–ocean model. *J. Atmos. Sci.*, **45**, 2889–2919.
- Bejarano, L., and F.-F. Jin, 2008: Coexistence of equatorial coupled modes of ENSO. *J. Climate*, **21**, 3051–3067.
- Clarke, A. J., 1994: Why are surface equatorial ENSO winds anomalously westerly under anomalous large-scale convection? *J. Climate*, **7**, 1623–1627.
- Davey, M., and Coauthors, 2002: STOIC: A study of coupled model climatology and variability in tropical ocean regions. *Climate Dyn.*, **18**, 403–420.
- Delworth, T. L., and Coauthors, 2006: GFDL’s CM2 global coupled climate models. Part I: Formulation and simulation characteristics. *J. Climate*, **19**, 634–674.
- Gill, A. E., 1982: *Atmosphere–Ocean Dynamics*. Academic Press, 662 pp.
- Gnanadesikan, A., and Coauthors, 2006: GFDL’s CM2 global coupled climate models. Part II: The baseline ocean simulation. *J. Climate*, **19**, 675–697.
- Griffies, S. M., and Coauthors, 2005: Formulation of an ocean model for global climate simulations. *Ocean Sci.*, **1**, 45–79.
- Gualdi, S., A. Navarra, E. Guilyardi, and P. Delecluse, 2003: Assessment of the tropical Indo-Pacific climate in the SINTEX CGCM. *Ann. Geophys.*, **46**, 1–26.
- Guilyardi, E., P. Delecluse, S. Gualdi, and A. Navarra, 2003: Mechanisms for ENSO phase change in a coupled GCM. *J. Climate*, **16**, 1141–1158.
- , and Coauthors, 2004: Representing El Niño in coupled ocean–atmosphere GCMs: The dominant role of the atmospheric component. *J. Climate*, **17**, 4623–4629.
- Hannachi, A., D. B. Stephenson, and K. R. Sperber, 2003: Probability-based methods for quantifying nonlinearity in the ENSO. *Climate Dyn.*, **20**, 241–256.
- Hoerling, M. P., A. Kumar, and M. Zhong, 1997: El Niño, La Niña, and the nonlinearity of their teleconnections. *J. Climate*, **10**, 1769–1786.
- Jin, F.-F., 1996: Tropical ocean–atmosphere interaction, the Pacific cold tongue, and the El Niño–Southern Oscillation. *Science*, **274**, 76–78.
- , 1997a: An equatorial ocean recharge paradigm for ENSO. Part I: Conceptual model. *J. Atmos. Sci.*, **54**, 811–829.
- , 1997b: An equatorial ocean recharge paradigm for ENSO. Part II: A stripped-down coupled model. *J. Atmos. Sci.*, **54**, 830–847.
- , 2001: Low-frequency modes of tropical ocean dynamics. *J. Climate*, **14**, 3874–3881.
- , and S.-I. An, 1999: Thermocline and zonal advection feedbacks within the equatorial ocean recharge oscillator model for ENSO. *Geophys. Res. Lett.*, **26**, 2989–2992.
- , J.-S. Kug, S.-I. An, and I.-S. Kang, 2003: A near-annual coupled ocean–atmosphere mode in the equatorial Pacific ocean. *Geophys. Res. Lett.*, **30**, 1080, doi:10.1029/2002GL015983.
- Kang, I.-S., S.-I. An, and F.-F. Jin, 2001: A systematic approximation of the SST anomaly equation for ENSO. *J. Meteor. Soc. Japan*, **79**, 1–10.
- Kao, H. Y., and J. Y. Yu, 2009: Contrasting eastern-Pacific and central-Pacific types of ENSO. *J. Climate*, **22**, 615–632.
- Kim, D., J.-S. Kug, I.-S. Kang, F.-F. Jin, and A. T. Wittenberg, 2008: Tropical Pacific impacts of convective momentum transport in the SNU coupled GCM. *Climate Dyn.*, **31**, 213–226, doi:10.1007/s00382-007-0348-4.
- Kug, J.-S., I.-S. Kang, and S.-I. An, 2003: Symmetric and antisymmetric mass exchanges between the equatorial and off-equatorial Pacific associated with ENSO. *J. Geophys. Res.*, **108**, 3284, doi:10.1029/2002JC001671.
- , B. P. Kirtman, and I.-S. Kang, 2006a: Interactive feedback between ENSO and the Indian Ocean in an interactive coupled model. *J. Climate*, **19**, 6371–6381.
- , T. Li, S.-I. An, I.-S. Kang, J.-J. Luo, S. Masson, and T. Yamagata, 2006b: Role of the ENSO–Indian Ocean coupling on ENSO variability in a coupled GCM. *Geophys. Res. Lett.*, **33**, L09710, doi:10.1029/2005GL024916.
- , S.-I. An, Y.-G. Ham, and I.-S. Kang, 2009a: Changes in El Niño and La Niña teleconnections over North Pacific–America in the global warming simulations. *Theor. Appl. Climatol.*, doi:10.1007/s00704-009-0183-0, in press.
- , F.-F. Jin, and S.-I. An, 2009b: Two types of El Niño events: Cold tongue El Niño and warm pool El Niño. *J. Climate*, **22**, 1499–1515.
- , K.-P. Sooraj, D. Kim, I.-S. Kang, F.-F. Jin, Y. N. Takayabu, and M. Kimoto, 2009c: Simulation of state-dependent high-frequency atmospheric variability associated with ENSO. *Climate Dyn.*, **32**, 635–648, doi:10.1007/s00382-008-0434-2.
- Larkin, N. K., and D. E. Harrison, 2005a: On the definition of El Niño and associated seasonal average U.S. weather anomalies. *Geophys. Res. Lett.*, **32**, L13705, doi:10.1029/2005GL022738.
- , and —, 2005b: Global seasonal temperature and precipitation anomalies during El Niño autumn and winter. *Geophys. Res. Lett.*, **32**, L16705, doi:10.1029/2005GL022860.
- Latif, M., and Coauthors, 2001: ENSIP: The El Niño simulation intercomparison project. *Climate Dyn.*, **18**, 255–276.
- Lau, N.-C., and M. J. Nath, 2004: Coupled GCM simulation of atmosphere–ocean variability associated with zonally asymmetric SST changes in the tropical Indian Ocean. *J. Climate*, **17**, 245–265.
- Lengaigne, M., and G. A. Vecchi, 2009: Contrasting the termination of moderate and extreme El Niño events in coupled general circulation models. *Climate Dyn.*, doi:10.1007/s00382-009-0562-3, in press.
- Lin, S.-J., 2004: A “vertically Lagrangian” finite-volume dynamical core for global models. *Mon. Wea. Rev.*, **132**, 2293–2307.
- Meinen, C. S., and M. J. McPhaden, 2000: Observations of warm water volume changes in the equatorial Pacific and their relationship to El Niño and La Niña. *J. Climate*, **13**, 3551–3559.
- , and —, 2001: Interannual variability in warm water volume transports in the equatorial Pacific during 1993–99. *J. Phys. Oceanogr.*, **31**, 1324–1345.

- Neelin, J. D., D. S. Battisti, A. C. Hirst, F.-F. Jin, Y. Wakata, T. Yamagata, and S. E. Zebiak, 1998: ENSO theory. *J. Geophys. Res.*, **103** (C7), 14 261–14 290.
- Picaut, J., F. Masia, and Y. du Penhoat, 1997: An advective-reflective conceptual model for the oscillatory nature of the ENSO. *Science*, **277**, 663–666.
- Rasmusson, E. M., and T. H. Carpenter, 1982: Variations in tropical sea surface temperature and surface wind fields associated with the Southern Oscillation/El Niño. *Mon. Wea. Rev.*, **110**, 354–384.
- Rodgers, K. B., P. Friederichs, and M. Latif, 2004: Tropical Pacific decadal variability and its relation to decadal modulations of ENSO. *J. Climate*, **17**, 3761–3774.
- Ropelewski, C. F., and M. S. Halpert, 1987: Global and regional scale precipitation patterns associated with the El Niño/Southern Oscillation. *Mon. Wea. Rev.*, **115**, 1606–1626.
- Timmermann, A., 2003: Decadal ENSO amplitude modulations: A nonlinear paradigm. *Global Planet. Change*, **37**, 135–156.
- Vecchi, G. A., B. J. Soden, A. T. Wittenberg, I. M. Held, A. Leetmaa, and M. J. Harrison, 2006: Weakening of tropical Pacific atmospheric circulation due to anthropogenic forcing. *Nature*, **441**, 73–76, doi:10.1038/nature04744.
- Wallace, J. M., E. M. Rasmusson, T. P. Mitchell, V. E. Kousky, E. S. Sarachik, and H. Von Storch, 1998: On the structure and evolution of ENSO-related climate variability in the tropical Pacific: Lessons from TOGA. *J. Geophys. Res.*, **103**, 14 169–14 240.
- Wang, C., 2000: On the atmospheric responses to tropical Pacific heating during the mature phase of El Niño. *J. Atmos. Sci.*, **57**, 3767–3781.
- , R. H. Weisberg, and J. I. Virmani, 1999: Western Pacific interannual variability associated with the El Niño–Southern Oscillation. *J. Geophys. Res.*, **104**, 5131–5149.
- Weisberg, R. H., and C. Wang, 1997: A western Pacific oscillator paradigm for the El Niño–Southern Oscillation. *Geophys. Res. Lett.*, **24**, 779–782.
- Weng, H., K. Ashok, S. K. Behera, S. A. Rao, and T. Yamagata, 2007: Impacts of recent El Niño Modoki on dry/wet conditions in the Pacific rim during boreal summer. *Climate Dyn.*, **29**, 113–129, doi:10.1007/s00382-007-0234-0.
- Wittenberg, A. T., A. Rosati, N.-C. Lau, and J. J. Ploshay, 2006: GFDL’s CM2 global coupled climate models. Part III: Tropical Pacific climate and ENSO. *J. Climate*, **19**, 698–722.
- Wu, R., and B. Kirtman, 2004a: Understanding the impacts of the Indian Ocean on ENSO variability in a coupled GCM. *J. Climate*, **17**, 4019–4031.
- , and B. P. Kirtman, 2004b: Biennial oscillation of the monsoon–ENSO system in an interactive ensemble coupled GCM. *J. Climate*, **17**, 1623–1640.
- Yeh, S.-W., J.-S. Kug, B. Dewitte, M.-H. Kwon, B. Kirtman, and F.-F. Jin, 2009: El Niño in a changing climate. *Nature*, **461**, 511–515.
- Yu, J.-Y., and C. R. Mechoso, 2001: Coupled atmosphere–ocean GCM study of the ENSO cycle. *J. Climate*, **14**, 2329–2350.
- , —, J. C. McWilliams, and A. Arakawa, 2002: Impacts of the Indian Ocean on the ENSO cycle. *Geophys. Res. Lett.*, **29**, 1204, doi:10.1029/2001GL014098.